Supplementary Information

Upcycling of Spent $LiFePO_4$ Cathodes to Efficient Oxygen Evolution Electrocatalysts in Anion Exchange Membrane Water Electrolysis

Baoling Niu[a], Huijing Ma[a], Xia Long[b], Xufang Qian[a*] and Yixin Zhao[a*]

[a] State Key Laboratory of Green Papermaking and Resource Recycling, School of Environmental Science and Engineering, Shanghai Jiao Tong University, Shanghai 200240, China

[b] China-UK Low Carbon College, Shanghai Jiao Tong University, Shanghai 200240, China

Corresponding Author:

E-mail: qianxufang@sjtu.edu.cn, yixin.zhao@sjtu.edu.cn.

EXPERIMENTAL DETAILS

Materials and reagents. Spent $LiFePO_4$ (R-LFP) powder and graphite (R-G) powder, which have been removed the binder, were purchased from Zhengzhou Guojuan Waste Batteries Recycling Company. Nickel nitrate hexahydrate ($Ni(NO_3)_2 \cdot 6H_2O$, 98%) and urea (99%) were purchased from Sinopharm Chemical Reagent Co., Ltd. KOH (95%), Isopropanol (99%) and IrO_2 (Ir750520) were purchased from Shanghai Macklin Biochemical Co., Ltd, Hipure Chem Co., Ltd and Yantai Yijia New Material Technology Co., Ltd. Pt/C (40 wt%), Nafion solution (5 wt.%) and anion exchange membrane (AEM, PiperION-A80-HCO3 and Sustainion X37-50) were provided by Suzhou Sinero Technology Co., Ltd. Carbon paper (HCP030P) was provided by SCI Materials Hub. Kmem-80 μm and Nickel felt was purchased from Kmem-tech Co., Ltd and Taixin Electrochemical Equipment Co., Ltd, respectively. All of the solutions were prepared with ultrapure water produced by MilliQ Water System. All chemicals were used as received.

Preparation of Catalysts. R-LFP, R-G, nickel nitrate, urea and water were uniformly mixed and ball-milled at 650 rpm for 2 h. The molar ratio of R-LFP, R-G, nickel nitrate and urea was 1: 13: 0.5: 1.5, and the solid-liquid ratio was 90 g/ L. After drying, the product was calcined at 800°C under an Ar atmosphere for 2h. After cooling to room temperature, $LFP_1G_{13}Ni_{0.5}Urea_{1.5}$ was obtained. $LFP_1G_xNi_yUrea_z$ was synthesized by adjusting the molar ratio of four reactants.

Materials characterizations. The crystal structures of catalysts were characterized utilizing Xray diffraction analysis (XRD, Lab XRD-6100 diffractometer with Cu Kα radiation) at a scanning rate of 5° min^{-1} over the range of 10° to 80°. X-ray photoelectron spectroscopy (XPS) analysis was performed using a Kratos AXIS Ultra DLD. The morphology characterizations were carried out by JEOL JSM-7800F scanning electron microscopy (SEM) and transmission electron microscopy (TEM, Thermo Scientific Talos F200X).

Electrochemical measurements. All electrochemical tests were performed using a standard three-electrode system at room temperature, with Hg/HgO and Pt mesh as the reference electrode and the counter electrode, respectively. Unless otherwise indicated, the voltage reported in this study was converted to the RHE reference scale by the following eq 1.

$$E\ (vs.\ RHE) = E\ (vs.\ Hg/HgO) + 0.098 + 0.059 \times pH \quad (1)$$

In order to prepare the working electrode, 10 mg of catalyst powder was dispersed in a 1: 1 volume ratio in a 900 uL mixed solvent of ultrapure water and isopropanol, and 100 μL of 5 wt% Nafion solution was added. After ultrasonication, crushing and stirring, a uniform catalyst slurry was obtained. Subsequently, 4 μL of catalyst ink was dropped on a glassy carbon electrode (RDE, 3 mm in diameter) to form a uniform catalyst coating. The OER polarization curve was tested in oxygen-saturated 1M KOH to fix the reversible oxygen voltage. It was tested at a scanning rate of 10 mV s^{-1} at 1600 rpm at ambient temperature, and the curve after reaching a stable state was recorded. The electrolyte resistance (R) was measured by the impedance test at 1.52 V (vs. RHE), with an amplitude of 5 mV and a frequency range of 10^{-2} - 10^{5} Hz. The iR compensation was calculated by eq 2.

$$E\ (vs.\ RHE) = E\ (vs.\ Hg/HgO) + 0.098 + 0.059 \times pH - 90\% \times iR \quad (2)$$

By plotting the relationship between the overpotential (η) and the logarithmic current (log (j)), the polarization curve was transformed into a Tafel curve. The Tafel slope (b) could be obtained by fitting the linear part of the Tafel curve according to eq 3.

$$\eta = b \log(j) + a \quad (3)$$

ECSA was estimated by measuring C_{dl} from the cyclic voltammograms curves tested in a non-Faradaic region at 0.9-1.0 V (vs. RHE) at various scan rates (20, 40, 60, 80, and 100 mV s^{-1}) using the equation:

$$ECSA = C_{dl} / C_s \quad (4)$$

where C_s is the specific capacitance of catalysts, which is usually 0.04 mF cm^{-2} for the flat surface.

The stability test was measured on CHI 760e (Chenhua). The working electrode was prepared by dropping the above catalyst slurry onto a nickel felt with a working area of 1 × 1cm, and the catalyst loading was 1mg cm^{-2}. Before each stability test, multiple LSV tests were firstly performed. After stabilization, the stability test was tested at 0.25A cm^{-2}.

AEMWE Measurements. $LFP_1G_{13}Ni_{0.5}Urea_{1.5}$, IrO_2, Pt/C and ionomer (Nafion solution) were dispersed in a mixed solvent (v_{H2O}:$v_{isopropanol}$ = 1: 13). Gas diffusion electrodes (GDEs) were prepared by spraying anode catalyst ink and cathode catalyst ink on nickel felt (1 × 1cm) and carbon paper (1 × 1cm), respectively. The catalyst loadings of the anode and cathode were 1 ± 0.2 mg cm^{-2} and 0.5 ± 0.2 mg cm^{-2}, respectively. Before AEMWE test, different kinds of AEM were immersed in 1 M KOH for one night and then replaced with fresh KOH solution. AEMWE tests were conducted at DH7000D (DongHua). The J-V curves were tested at a scanning rate of 10 mV s^{-1} and a KOH flow of 70 ml min^{-1}. EIS tests were conducted at a range of 10^{-1} - 10^5 Hz, an amplitude of 50 mA, and a current of 0.5 A (The applied RMS AC was 10% of the corresponding DC). EIS and durability tests were performed at 80 ℃ and 60 ℃, seperately. The KOH flow of durability tests was 20 ml min^{-1}.

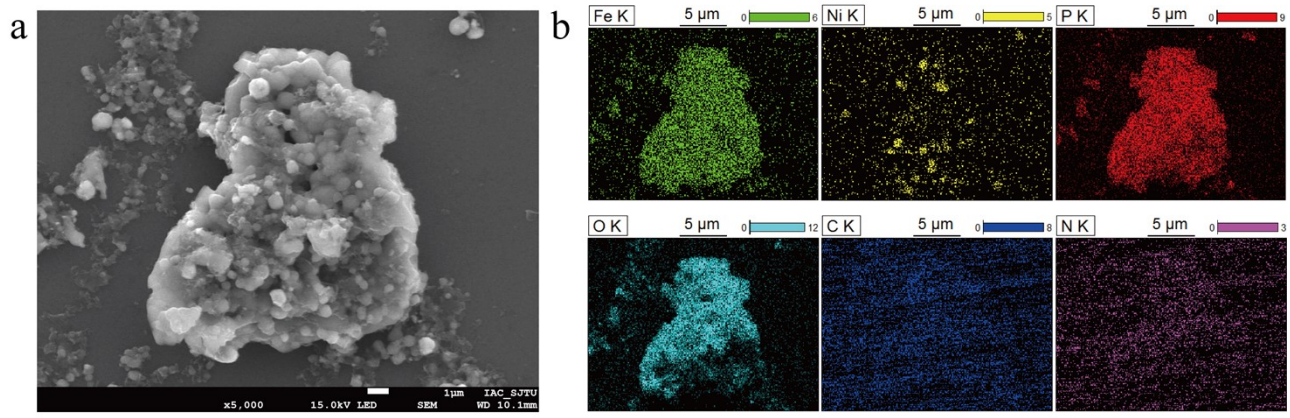

Figure S1. (a) SEM and (b) the corresponding EDS mapping images of $LFP_1G_{13}Ni_{0.5}Urea_{1.5}$.

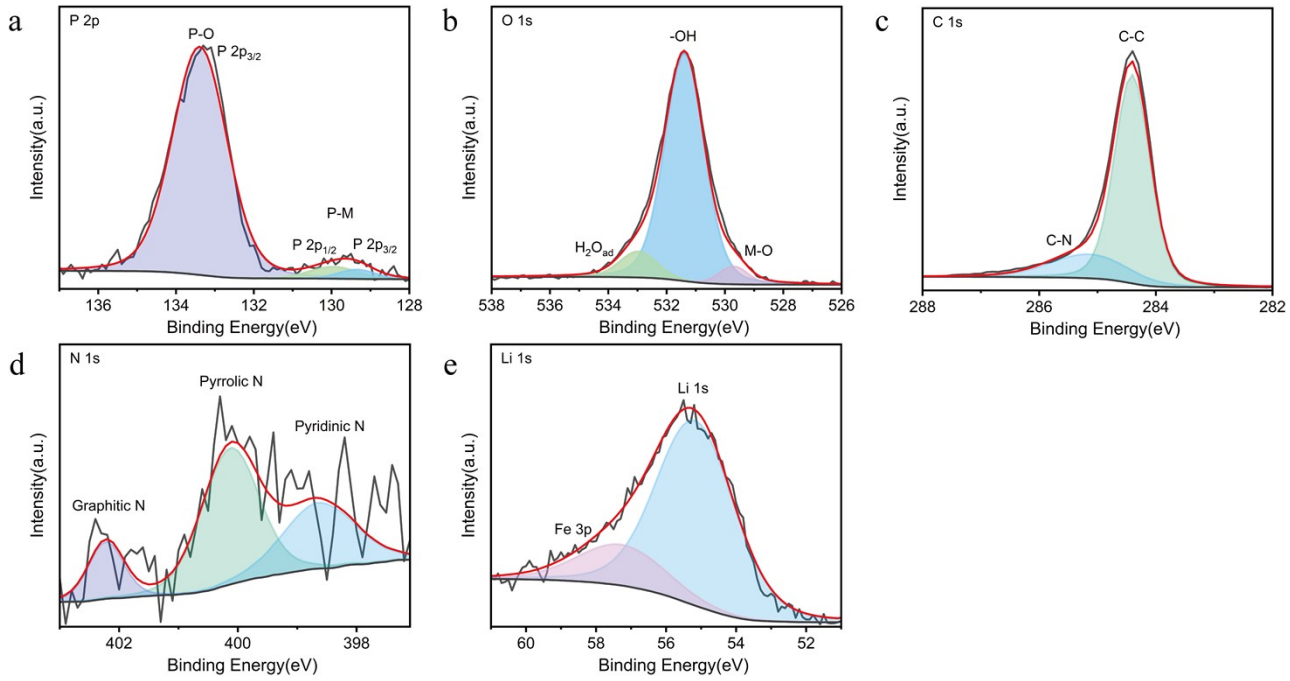

Figure S2. (a) P 2p spectra, (b) O 1s spectra, (c) C 1s spectra, (d) N 1s spectra and (e) Li 1s spectra of $LFP_1G_{13}Ni_{0.5}Urea_{1.5}$.

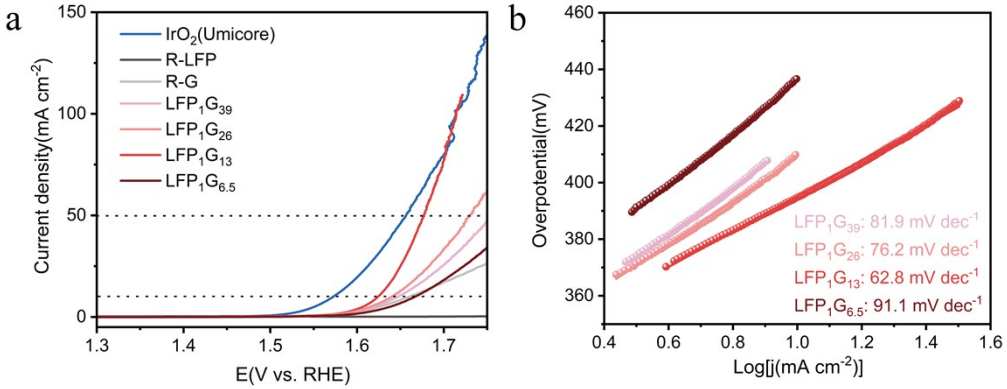

Figure S3. (a) LSV curves, (b) Tafel slopes of different electrocatalysts in $n_{R\text{-}LFP}$: $n_{R\text{-}G}$ optimization experiment.

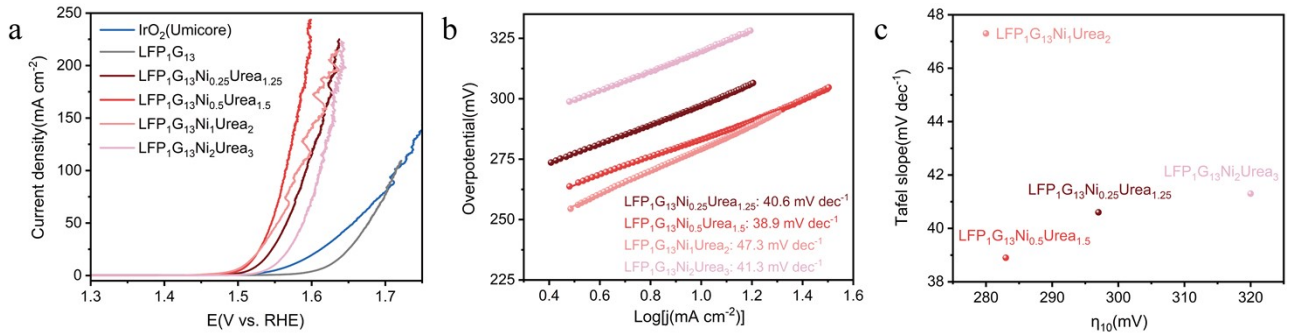

Figure S4. (a) LSV curves, (b) Tafel slopes, (c) comparison of overpotential and Tafel slope of different electrocatalysts in n_{Fe}: n_{Ni} optimization experiment with n_{Urea}:(n_{Fe}+n_{Ni}) of 1:1.

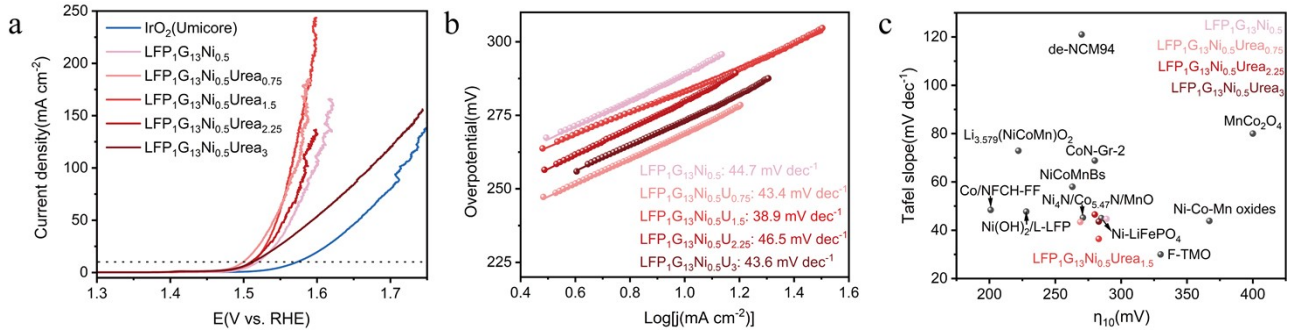

Figure S5. (a) LSV curves, (b) Tafel slopes, (c) comparison of overpotential and Tafel slope of different electrocatalysts in n_{Urea}: (n_{Fe}+n_{Ni}) optimization experiment.

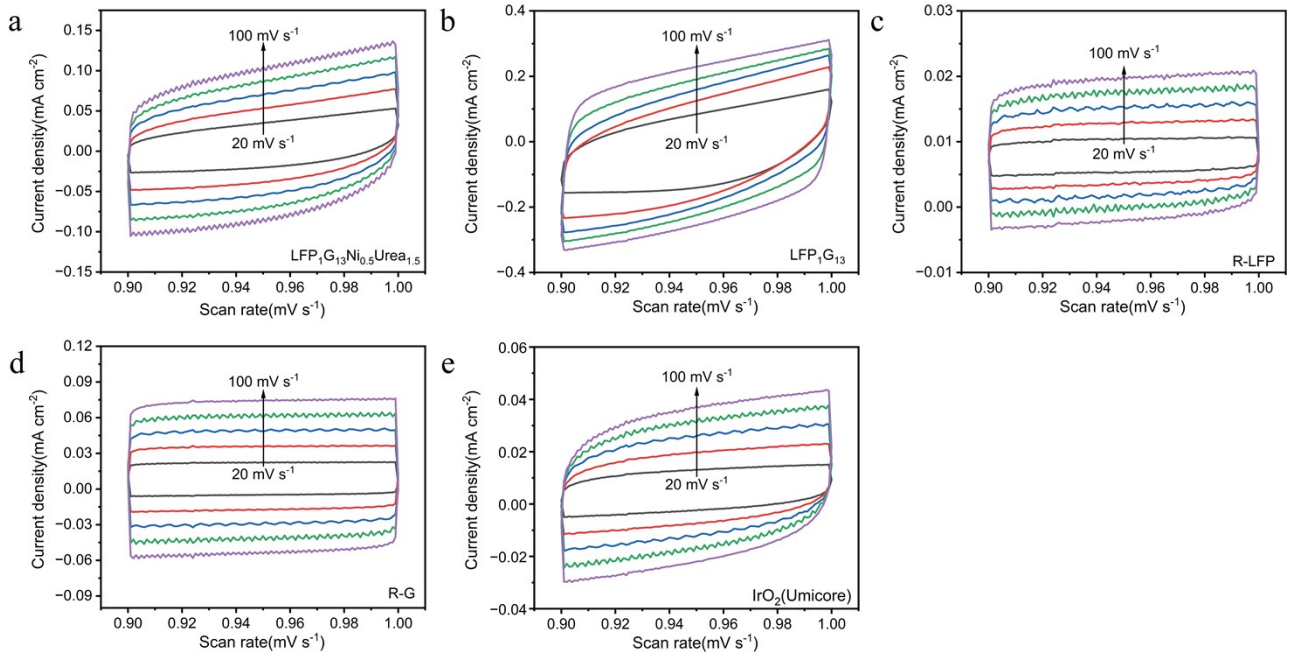

Figure S6. Cyclic voltammograms curves at the non-Faradic potential scope. (a) $LFP_1G_{13}Ni_{0.5}Urea_{1.5}$, (b) LFP_1G_{13}, (c) R-LFP, (d) R-G, (e) IrO_2.

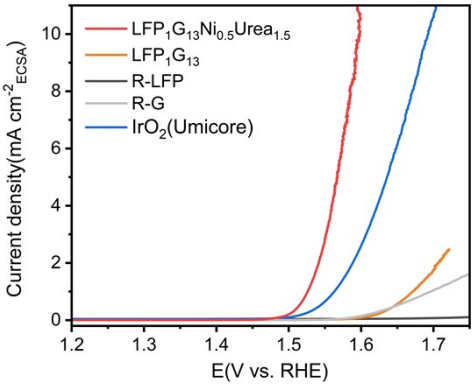

Figure S7. ECSA-normalized LSV curves of electrodes.

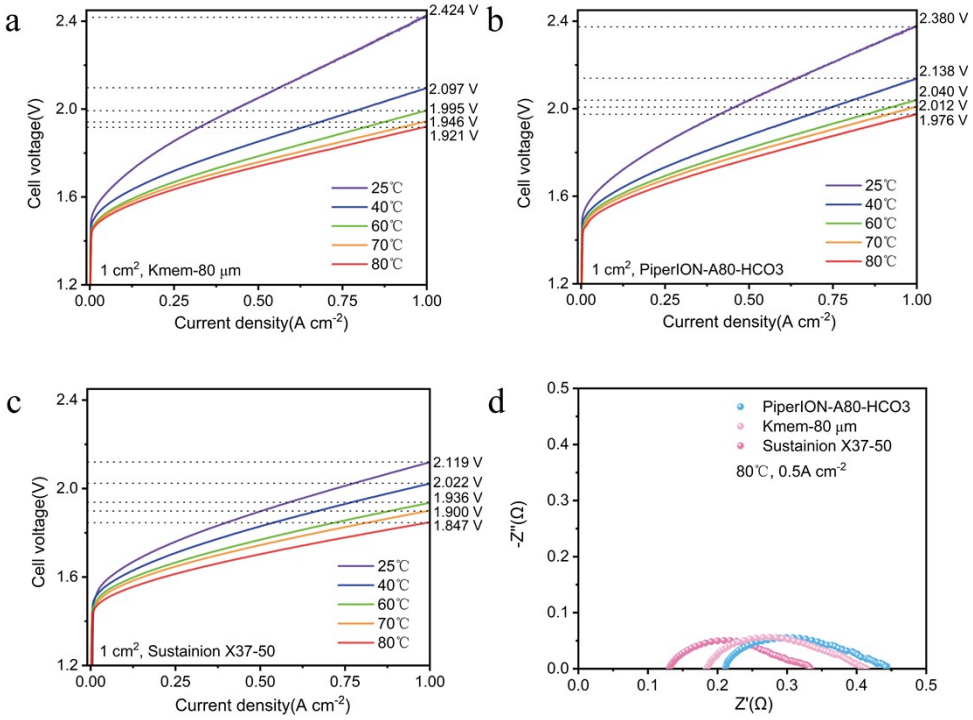

Figure S8. J-V curves of $LFP_1G_{13}Ni_{0.5}Urea_{1.5}^{(+)}||Pt/C^{(-)}$ with (a) Kmem-80 μm, (b) PiperION-A80-HCO3, (c) Sustainion X37-50 (without iR correction), (d) Nyquist plots of $LFP_1G_{13}Ni_{0.5}Urea_{1.5}^{(+)}||Pt/C^{(-)}$ with different membranes.

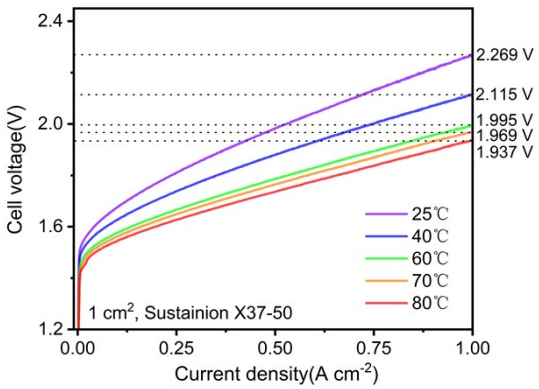

Figure S9. J-V curves of $IrO_2^{(+)}||Pt/C^{(-)}$ (without iR correction).

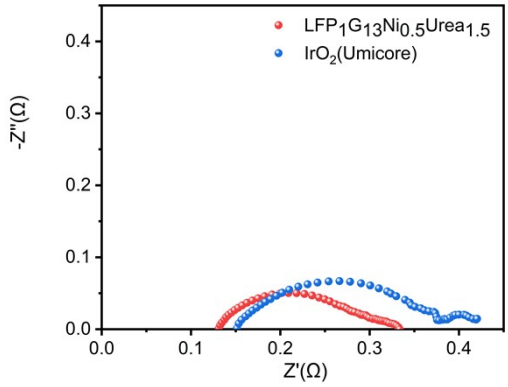

Figure S10. Nyquist plots of $LFP_1G_{13}Ni_{0.5}Urea_{1.5}^{(+)}||Pt/C^{(-)}$ and $IrO_2^{(+)}||Pt/C^{(-)}$.

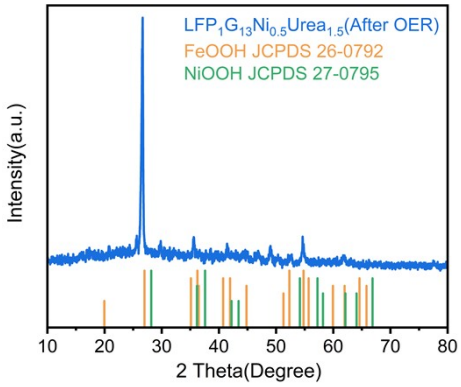

Figure S11. XRD pattern of $LFP_1G_{13}Ni_{0.5}Urea_{1.5}$ after OER.

Table S1. The fitting results of Nyquist plots according to the equivalent circuit model.

Catalysts	R_s (Ω)	R_{ct} (Ω)
$LFP_1G_{13}Ni_{0.5}Urea_{1.5}$	12.8	85.3
LFP_1G_{13}-2	42.9	2209.0
R-LFP	22.9	2613.0
R-G	33.8	1869.0
IrO_2	15.3	302.9

Table S2. Comparison of OER performance between $LFP_1G_{13}Ni_{0.5}Urea_{1.5}$ and state-of-the-art catalysts upgraded from waste LIBs.

Cathode material	OER catalysts	η_{10} (mV)	Tafel slope (mV dec^{-1})	OER stability	AEMWE performance	AEMWE stablity	Ref.
LFP	Ni-$LiFePO_4$	285	45	14 h, 10 mA cm^{-2} (1 M KOH)	/	/	1
LFP	$Ni(OH)_2$/L-LFP	228	47.7	1000 h, 0.1 A cm^{-2} (1 M KOH); 600 h, 0.1 A cm^{-2} (1 M KOH + seawater)	60℃, 1 A/cm^{-2}, 2.7 V (6M KOH + seawater)	60℃, 0.25 A cm^{-2}, 100 h (6M KOH + seawater)	2
NCM523	Ni-Co-Mn Oxides	36.7	43.84	8.5 h, 10 mA cm^{-2} (1 M KOH)	/	/	3
NCM523	$Ni_4N/Co_{5.47}N$/ MnO	271	45.21	140 h, 160 mA^{-2} (1 M KOH)	/	/	4
NCM622	Co/NFCH-FF	201	48.4	190 h, 50 mA cm^{-2} (1 M KOH)	/	/	5
NCM6 series	F-TMO	330	30	/	70℃, 3 A/cm^{-2}, 2.56 V (pure water）	70℃, 0.5 A cm^{-2}, 336 h (pure water）	6
NCM811	NiCoMnBs	263	57.98	12 h, 10 mA cm^{-2} (1 M KOH)	/	/	7
NCM811	$Li_{3.579}$ (NiCoMn) O_2	222	72.9	25 h, 100 mA cm^{-2} (1 M KOH)	/	/	8

Table S1. continued

Cathode material	OER catalysts	η_{10} (mV)	Tafel slope (mV dec^{-1})	OER stability	AEMWE performance	AEMWE stablity	Ref.
NCM94	de-NCM94	270	121	300 h, 10 mA cm^{-2} (1 M KOH)	/	/	[9]
LCO	CoN-Gr-2	280	68.83	10 h, 1.6 V (1 M KOH)	/	/	[10]
LCO+LMO	$MnCo_2O_4$	400	80	16.7 h, 1.54V-1.645 V (1 M KOH)	/	/	[11]
LFP	$LFP_1G_{13}Ni_{0.5}Urea_{1.5}$	283	38.9	110 h, 250 mA^{-2} (1 M KOH)	80℃, 1 A cm^{-2}, 1.847 V (1M KOH)	60℃, 0.5 A cm^{-2}, 800 h (1M KOH)	This work

Table S3. AEMWE performance summary of AEM membrane type optimization.

Types of AEM membrane	Thickness of AEM membrane	Catalyst loading method	E_{cell} (60℃)	E_{cell} (80℃)
PiperION-A80-HCO3	80 μm	catalyst-coated substrate	2.040 V	1.976 V
Kmem-80 μm	80 μm	catalyst-coated substrate	1.995 V	1.921 V
Sustainion X37-50	50 μm	catalyst-coated substrate	1.936 V	1.847 V

Table S4. Comparison of AEMWE electrolyzer performance in the reported literatures in 1 M KOH.

Electrode (anode || cathode)	E_{cell} (60℃)	E_{cell} (80℃)	AEMWE stability	Ref.
MOF@POM||Pt/C	1.62	1.58	2000 h (60 ℃, 2 A cm^{-2})	[12]
CAPist-L1||Ni_4Mo/MoO_2	1.63	1.57	1500 h (80 ℃, 1 A cm^{-2})	[13]
Cs^+-NiFeOOH NS||PtRu/C	1.7	1.541	450 h (60 ℃, 1 A cm^{-2})	[14]
NiFeLDH||Pt/C	1.72	1.63	110 h (60 ℃, 1 A cm^{-2}) 110 h (80 ℃, 1 A cm^{-2})	[15]
NiFe/ATNT||Pt/C/ATNT	1.76	1.71	1500 h (80 ℃, 0.5 A cm^{-2})	[16]
NDCO||Pt/C	1.78	/	325 h (60 ℃, 1 A cm^{-2})	[17]
Ni(Fe) MOF||$NiMoO_x$	1.79	/	300 h (60 ℃, 0.5 A cm^{-2}) 170 h (60 ℃, 1 A cm^{-2})	[18]
$Ce_{0.1}$-Fe_2P/NiCoP || $Ce_{0.1}$-CoP/Ni_3P	1.812	/	579 h (60 ℃, 1 A cm^{-2})	[19]
$CoCrO_x$||Pt/C	1.93	/	120 h (60 ℃, 0.5 A cm^{-2})	[20]
Fe/S-NiOOH/NF||Pt/C	2.24	/	100 h (60 ℃, 1 A cm^{-2})	[21]
NiFe_FA_NN||NiFe_FA_NN	2.32	/	200 h (60 ℃, 0.5 A cm^{-2})	[22]
$LFP_1G1_3Ni_{0.5}Urea_{1.5}$||Pt/C	1.936	1.847	800 h (60 ℃, 0.5 A cm^{-2})	This work

Note: The E_{cell} represented the voltage at a current density of 1A cm^{-2}.

References

1. B. H. Cui, C. Liu, J. F. Zhang, J. J. Lu, S. L. Liu, F. S. Chen, W. Zhou, G. Y. Qian, Z. Wang, Y. D. Deng, Y. N. Chen and W. B. Hu, *Science China-Materials*, 2021, **64**, 2710-2718.
2. Z. Li, M. T. Li, Y. Q. Chen, X. C. Ye, M. J. Liu and L. Y. S. Lee, *Angewandte Chemie-International Edition*, 2024, **63**.
3. F. Balqis, Y. Irmawati, D. S. Geng, F. A. A. Nugroho and A. Sumboja, *Acs Applied Nano Materials*, 2023, **7**, 18138-18145.
4. H. F. Jiang, R. R. Wang, H. H. Liu, Q. Q. Liu, M. Cheng, W. J. Ma, J. Hu, T. Wei, Z. D. Meng, B. Liu, M. Z. Chen and W. F. Li, *International Journal of Hydrogen Energy*, 2025, **121**, 22-30.
5. L. Yu, H. H. Chen, G. Y. Ma, J. R. Zeng, Y. Liu, G. W. Zhang, L. B. Zhong and Y. J. Qiu, *Journal of Colloid and Interface Science*, 2024, **668**, 190-201.
6. L. Y. Zhang, Q. C. Xu, S. T. Wen, H. X. Zhang, L. Chen, H. Jiang and C. Z. Li, *Acs Nano*, 2024, **18**, 22454-22464.
7. Z. J. Chen, W. S. Zou, R. J. Zheng, W. F. Wei, W. Wei, B. J. Ni and H. Chen, *Green Chemistry*, 2021, **23**,

6538-6547.
8. L. N. Jia, G. H. Du, D. Han, Y. T. Wang, W. Q. Zhao, S. X. Chen, Q. M. Su and B. S. Xu, *Journal of Colloid and Interface Science*, 2024, **653**, 246-257.
9. S. J. Li, X. M. Zhu, X. H. Wang, W. S. Luo, X. Yu, Q. Y. Guo, K. M. Song, H. Tian, X. Z. Cui and J. L. Shi, *Materials Chemistry Frontiers*, 2023, **7**, 5868-5878.
10. T. T. Liu, S. Cai, G. F. Zhao, Z. H. Gao, S. M. Liu, H. N. Li, L. J. Chen, M. A. Li, X. F. Yang and H. Guo, *Journal of Energy Chemistry*, 2021, **62**, 440-450.
11. S. Natarajan, S. Anantharaj, R. J. Tayade, H. C. Bajaj and S. Kundu, *Dalton Transactions*, 2017, **46**, 14382-14392.
12. K. H. Yue, R. H. Lu, M. B. Gao, F. Song, Y. Dai, C. F. Xia, B. B. Mei, H. L. Dong, R. J. Qi, D. L. Zhang, J. W. Zhang, Z. Y. Wang, F. Q. Huang, B. Y. Xia and Y. Yan, *Science*, 2025, **388**, 430-436.
13. Z. H. Li, G. X. Lin, L. Q. Wang, H. Lee, J. Du, T. Tang, G. H. Ding, R. Ren, W. L. Li, X. Cao, S. W. Ding, W. T. Ye, W. X. Yang and L. C. Sun, *Nature Catalysis*, 2024, **7**, 944-952.
14. S. H. Wang, Q. Jiang, C. Hu, H. Y. Zhang, R. H. Feng, C. R. Zhang, C. S. Hsu, C. P. Guo, H. M. Chen, Y. M. Lee, D. Zhang and F. Song, *Nature Synthesis*, 2025, **4**, 1308-1318.
15. M. Klingenhof, H. Trzesniowski, S. Koch, J. Zhu, Z. Zeng, L. Metzler, A. Klinger, M. Elshamy, F. Lehmann, P. W. Buchheister, A. Weisser, G. Schmid, S. Vierrath, F. Dionigi and P. Strasser, *Nature Catalysis*, 2024, **7**, 1213-1222.
16. S. Shaik, J. Kim, M. K. Kabiraz, F. Aziz, J. Y. Park, B. R. Anne, M. F. Li, H. W. Huang, K. M. Nam, D. Jo and S. I. Choi, *Nano-Micro Letters*, 2025, **17**.
17. P. C. Yu, X. L. Zhang, T. Y. Zhang, X. Y. N. Tao, Y. Yang, Y. H. Wang, S. C. Zhang, F. Y. Gao, Z. Z. Niu, M. H. Fan and M. R. Gao, *Journal of the American Chemical Society*, 2024, **146**, 20379-20390.
18. Y. Li, L. Yang, X. L. Hao, X. P. Xu, L. L. Xu, B. Wei and Z. W. Chen, *Angewandte Chemie-International Edition*, 2025, **64**.
19. F. Zhang, K. Wang, H. Zhang, S. L. Yang, M. Xu, Y. He, L. C. Lei, P. F. Xie and X. W. Zhang, *Advanced Functional Materials*, 2025, **35**.
20. S. C. Li, T. Liu, W. Zhang, M. Z. Wang, H. J. Zhang, C. L. Qin, L. L. Zhang, Y. D. Chen, S. W. Jiang, D. Liu, X. K. Liu, H. J. Wang, Q. Q. Luo, T. Ding and T. Yao, *Nature Communications*, 2024, **15**.
21. F. L. Wang, J. L. Tan, Z. Y. Jin, C. Y. Gu, Q. X. Lv, Y. W. Dong, R. Q. Lv, B. Dong and Y. M. Chai, *Small*, 2024, **20**.
22. Z. M. Wei, M. W. Guo and Q. B. Zhang, *Applied Catalysis B-Environment and Energy*, 2023, **322**.